THE IMPACT OF ATMOSPHERIC STABILITY ON HELICAL WAKE BEHIND A ROTATING BLADE: THE PHYSICS OF HELICAL VORTEX CORE IN PHYSICAL SPACE. (PART 1)

N.M. Zahari[1], L. Gan[2] and X. Mao[3]

[1]Faculty of Mechanical Engineering,
Universiti Teknikal Malaysia Melaka, Hang Tuah Jaya, 76100 Durian Tunggal, Melaka, Malaysia.

[2]Department of Engineering,
Durham University, Durham, DH1 3LE, UK

[3]Faculty of Engineering,
University of Nottingham, Nottingham, NG7 2RD, UK

Corresponding Author's Email: [1]normazlin@utem.edu.my

Article History: Received 31 December 2025; Revised 13 April 2026; Accepted 29 June 2026

ABSTRACT: *As wakes can be damaging to wind turbine structures and detrimental to their power generation, it is essential to study the wake development to prevent the undesirable wake impacts. A fundamental study on the breakdown mechanisms of a helical flow is conducted where the helical flow shares common traits with the wind turbine wake flow. The simulation data generated by a Direct Numerical Simulation (DNS) of flow around a rotating blade in a thermally stratified atmosphere were analyzed to investigate the impact of atmospheric thermal stability on wind-turbine wakes. A few of vortex identification techniques were presented, and the decision to carry out the following study using the vorticity magnitude, $|\varpi|$ was made. There is some interesting characteristics of the wake flow identified, such as its deformation/distortion, vorticity dynamics, vortex breakdown, and the centroid of the cores. All these analyses were focused only on the tip vortices.*

KEYWORDS: *Wake Flow; Helical Wake Flow; Wind Turbine Wake Flow; Atmospheric Thermal Stability, Vortex Identification.*

1.0 INTRODUCTION

In different kinds of flows, helical vortices are observed and found in nature and countless industrial applications. In rotating equipment such as propellers, wind turbines, and so forth they are often developed as tip vortices as depicted by some real-life events in Figure 1. This kind of flow has been the topic of numerous theoretical, experimental and numerical studies, for instance, the study in the wake of helicopters [1], propellers [2] or wind turbines [3] in which a complex system of vortices is shed possessing the features of general three-dimensional flows. These flows are discovered to be somewhat easier: they fulfil a helical symmetry at least locally, i.e., by combining axial translation and rotation, these vortices are invariant.

The vortex sheet of the flow behind the rotor system was created by the lift distribution along with the blades. A roll-up process sets in immediately after the vortex sheet is developed due to the interaction between the vortex components, which in the instant near-wake behind the rotor forms powerful tips and root vortices. The roll-up process is governed in essence by Biot–Savart's interaction law. The tip/root vortex system in most cases is unstable, eventually breaking down and forming small-scale turbulence further downstream owing to multiple instability mechanisms. What more complicated is the structure of the vortex sheet downstream a rotating wind turbine blade. The wake obtains a typical helical shape due to both rotational and axial velocity components. It is noted that the trailing vortex filaments follow a circular path.

Figure 1: Helical vortices created from different devices such as from a: (a) propeller [4]; (b) wing [5]; (c) rotor [6]; and (d) blade [7].

In the context of flow over a turbine blade, the occurrence of flow over a blunt body was discussed by Matin in her work [8], leading to vortex shedding. Figure 2 shows the development of distinct vortices in near-wake regions to large-scale structures in the far wake that form through the process of vortex pairing and stretching [9].

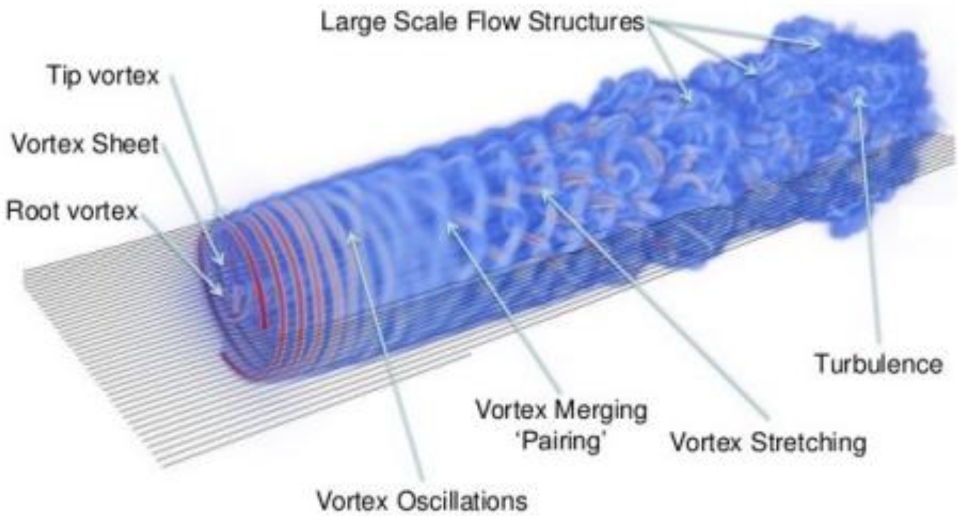

Figure 2: Evolution of a Wind Turbine Wake. Image is taken from [9]

2.0 THE GOVERNING EQUATIONS

In this study, DNS of helical wake flow behind a rotating blade in neutral (N), weakly stable (WS), and strongly stable (SS) stratification were performed at Re = 1000, and Re = 2000 defined as $Re = \frac{U_\infty D}{\upsilon}$ where U_∞ is the free-stream velocity, D is the radius of the rotating blade, and υ is the kinematic viscosity. The thermal stratification of the atmosphere will be described

ISSN 2180-1053 e-ISSN 2289-8123 Vol.18 No.1

in detail at the end of the next subsection.

The following dimensional equations are the continuity and momentum equation that has been derived from the incompressible Navier-Stokes equations:

$$\nabla \cdot u = 0 \tag{1}$$

$$\partial_t u + u \cdot \nabla u + \nabla p - Re^{-1} \nabla^2 u + T_s g = 0 \tag{2}$$

$$\partial_t T + u \cdot \nabla T - Re^{-1} \overset{-1}{\mathrm{Pr}} \nabla^2 T = 0 \tag{3}$$

where u, T, p, g, T_s and Re represent the dimensionless velocity flow, time, pressure, gravity term, thermal term, and Reynolds number, respectively. Meanwhile, Pr is Prandtl number given by $Pr = \frac{v}{\alpha}$ where α is thermal diffusion and $T_s = 1 - \beta(T - T_{ref})$ with the reference temperature, $T_{ref} = 298K$.

Dirichlet boundary condition specifies the value of a variable at a boundary. It may also be referred to as a fixed boundary condition. Therefore, it is used when a value needs to be imposed at a boundary. Typically, this study is dealt with a Dirichlet condition where the velocity is fixed at the inlet and the pressure is fixed at the outlet. Noted also, the rotational speed is constant for all the computations, $\Omega = 5rad/s$.

3.0 COMPUTATIONAL MODEL OF HELICAL FLOW BEHIND A ROTATING BLADE

Three-dimensional numerical simulations have been performed in cylindrical coordinate system with z, r and θ representing the streamwise, radial, and azimuthal coordinates, respectively, is adopted to study the flow behind the rotating blade. The computational domain, as shown in Figure 3 is a cylinder with dimensions$L_z = 63$, $L_r = 35$, where $-3 < z < 60$, $0 < r < 35$ respectively, and a rotating blade is located at $(z, r) = (0, 0)$. The computational domain then was normalized by D .

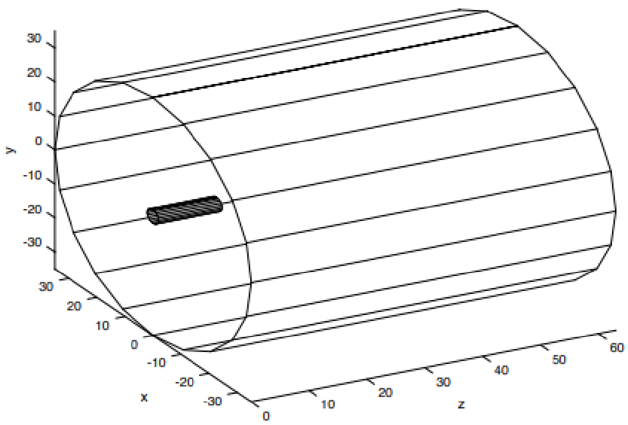

Figure 3: Schematic of the computational domain along the streamwise.

The sub-domain of the complete computational domain was being considered to perform the analysis in order to decrease the size of the computations and concentrate on the interesting part appropriate to the physics in the flow. In the sub-domain $1 < z < 11$, the perturbation growth is linear and the magnitude of the velocity of the perturbations remain low compared to the base flow. The non-linear effects in the wake breakdown and the turbulent wake are out the sub-domain. Thus, the analysis has been performed to the three components of the instantaneous velocity, (u, v, w) in a smaller region of the computational domain as shown in Figure 3.

The wake behind a wind turbine is typically divided into two sections; near wake and far wake, where it is difficult to determine exactly the boundary between the two sections. Nevertheless, it is known that the end of the near wake is where the shear layer hits the wake axis [10]. Crespo et al. [11] concluded that this normally takes place at around $2-5D$. The velocity deficit declines slowly downstream of the turbine in the far wake, and the wake is fully developed. Consequently, axis-symmetry and thus a self-similar wake structure can be assumed [10].

Figure 4 was referred for the view of Figure 3 in $zy-$ plane. This is to focus on the smaller domain which were studied in this work.

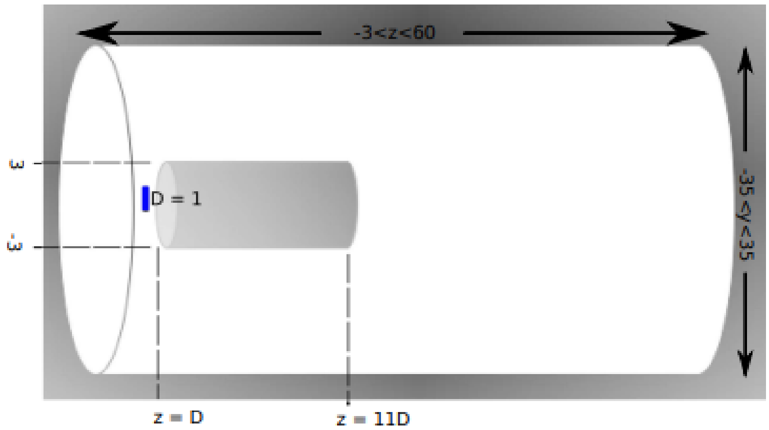

Figure 4: The side view of Figure 3 with the blue rectangle represents the radius of the rotating blade, $D = 1$, located at $(z, y) = (0, 0)$.

The atmospheric lapse rate, ζ refers to the change of an atmospheric variable with altitude transition. Lapse rates are typically expressed as the amount of temperature change associated with a specified amount of altitude change, such as 9.8° Kelvin (K) per kilometre or the equivalent 0.0098° K per meter. The lapse rate can be expressed as a negative number if the ambient air cools with increasing altitude. If the air heats at higher altitudes, the lapse rate then can be expressed as a positive number [12].

Atmospheric stability is atmospheric resistance to vertical air movement. A very stable atmosphere is one which has very little, if any, vertical air movement while a stable atmosphere is one which discourages vertical motion but has some air movement. On the other hand, an unstable atmosphere is one that promotes constant upward or downward vertical motion of the air. A neutral environment is one that neither discourages nor facilitates vertical air movement, and is also called conditionally stable. The stability depends on how the temperature of the air varies with altitude (the lapse rate of temperature).

In this study, all four atmospheric stability conditions were defined by setting their temperature field as given by (5) and illustrated in Figure 5.

$$T = \frac{y}{c} \tag{5}$$

with $-3 < y < 3$ and $c = 0,\ 200,\ 500,\ 1000$ for N, SS1, SS2 and WS, respectively.

When the temperature increases with altitude, a temperature inversion. Air is negatively buoyant at ground level and does not grow. If air is forced to rise, it will sink back towards the ground again. This is when the atmospheric condition is said to be in a strongly stable. In the present study, the lapse rates for both SS1 and SS2 as can be calculated from Figure 3.2(a) & Figure 3.2(d) is $\zeta_{SS1} = 0.001$, and $\zeta_{SS2} = 0.002$, respectively. In Figure 3.2(b), it shows that the temperature is the same as the dry adiabatic lapse rate with $\zeta_N = 0$. i.e., if air is forced to rise, it will cool at the same rate as the temperature around it drops. In this case, it will be neutrally buoyant and categorized as neutral. Last but not least, Figure 3.2(c) shows how the atmospheric stability was classified as weakly stable. It is when the temperature lapse rate is less than the dry adiabatic lapse rate (i.e. it falls less than by $0.0098°$ K), but temperature does decrease with altitude. In this study, $\zeta_{WS} = 0.005$.

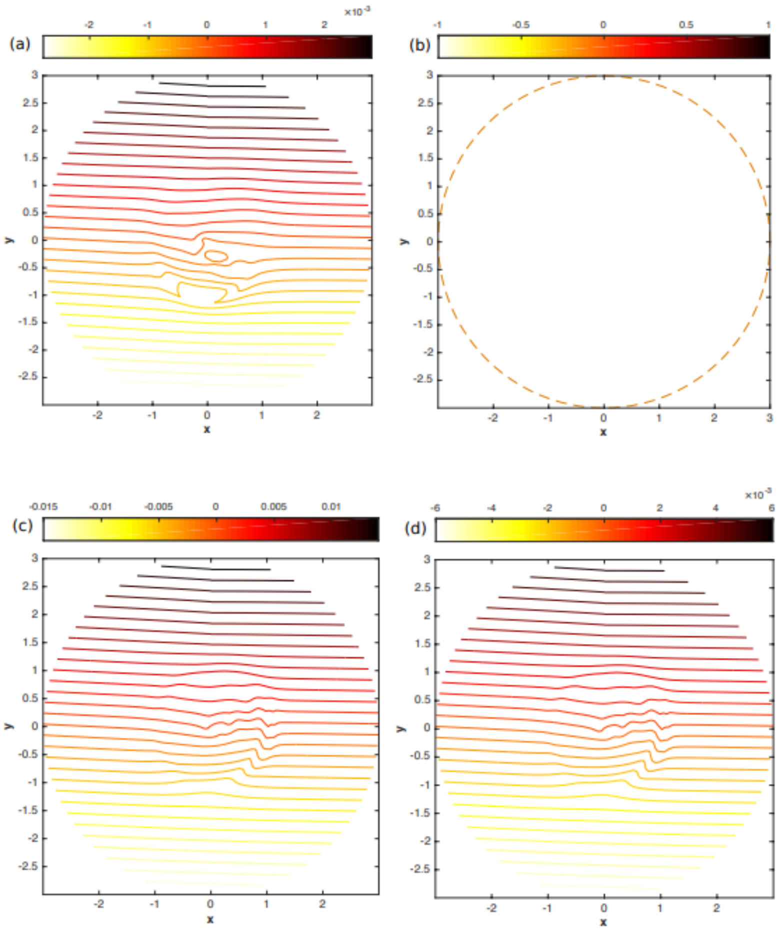

Figure 5: Temperature contours of: (a) SS1, (b) N, (c) WS, and (d) SS2 in the $xy-$ plane at $z = 5.5$.

4.0 RESULTS AND DISCUSSION

Wakes originate from the shed trailing vortices of the spinning blades that form the concentrated helical tip and root vortex structures. In considering the effect of upstream turbines on downstream turbines, the growth and lifetime of tip vortices are being the subjects of interest. Due to self-induced instability and ambient atmospheric turbulence, the tip vortices break up. Therefore, when considering the aerodynamic loads and fatigue on impacted turbines, the lifetime of tip vortices and the process of the break up is valuable knowledge. For this reason, [13] conducted a study focusing on the stability properties of tip vortices and the mechanisms leading to vortex pairing.

4.1 Vortex Identification

Vorticity is defined as the curl of the velocity by the following equation:

$$\varpi = \nabla \times u \tag{6}$$

where ∇ is the del operator and u is the flow velocity. Since it is equal to the rotation of the fluid at $(x,\ t)$, it can be used directly to identify vortices.

The vorticity tells how the velocity vector changes when one moves in a direction perpendicular to it, through an infinitesimal distance. It can be readily visualized by plotting the isosurfaces of vorticity magnitude, $|\varpi|$ given by the following equation, in which was commonly used for representing vortex cores. [14-16].

$$|\varpi| = \left(\varpi_x{}^2 + \varpi_y{}^2 + \varpi_z{}^2\right)^{\frac{1}{2}} \tag{7}$$

where ϖ_x, ϖ_y, ϖ_z is the vorticity of its three components.

Figure 6 shows the isosurface of $|\varpi|$ for Strongly Stable at Re = 1000 case (SS1, Re1k) and all the other cases which are SS1 at Re = 2000 (SS1, Re2k), Strongly Stable case 2 at Re = 1000 (SS2, Re1k), Weakly Stable at Re = 1000 (WS, Re1k), and Neutral at Re = 1000 and Re = 2000 (N, Re1k, and N, Re2k, respectively).

In particular, the tip and root vortices may interact depending on the tip speed ratio. However, the root vortices break down faster than the tip vortices as it can be seen in Figure7, due to their weak proximity. The root vortices are therefore not included in this analysis as there is a very weak interaction between root and tip vortices.

4.2 Deformation of the Helical Wake Flow

In this study, the deformation of the flow structure was defined to be the degree of eccentricity (non-circularity) the helical wake is. In order to quantify it, we average through slices of $|\varpi|$ in the streamwise direction over a range where the helical core makes a complete revolution (from now it will be called as 'cycle') as shown in Figure 8.

The available streamwise distance $1 < z < 11$ typically accommodates nine complete cycles, as shown in Figure 9. In each sub-figure, the black circle was plotted from the mean distance, $\bar{d}$ (which will be described later in the next paragraph) and the red circle with $r = 1.5$ were plotted for indicative purposes, to show qualitatively how non-circular the wake is.

The root-mean-square (RMS) error of the distance between the core points to the origin, d for observations of the mean distance, $\bar{d}$ was computes for $N = 9$ complete cycles (as shown in Figure 9 (a) – (i)) as the square root of the mean of the square of the deviations:

$$RMS = \sqrt{\sum_{i=1}^{N} \frac{(d_i - \bar{d}_i)^2}{N}} \tag{8}$$

A total of 100 core points was referred to the points with the highest values of $|\varpi|$ (after this will be called as the "core points") that formed the helical core structure of $|\varpi|$.

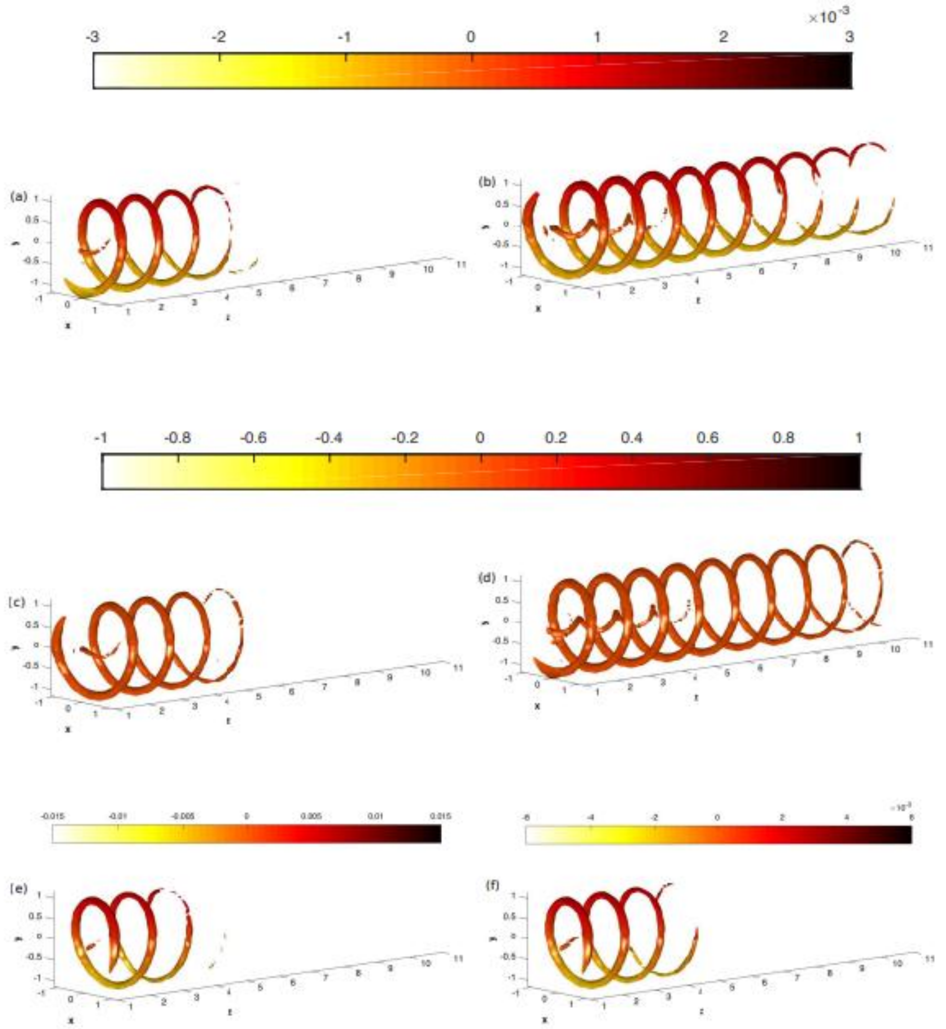

Figure 6: Isosurface of $|\varpi| = 2.5$ for: (a) SS1, Re1k, (b) SS1, Re2k, (c) N, Re1k, (d) N, Re2k, (e) WS, Re1k, and (f) SS2, Re1k cases with contours indicate their temperature field.

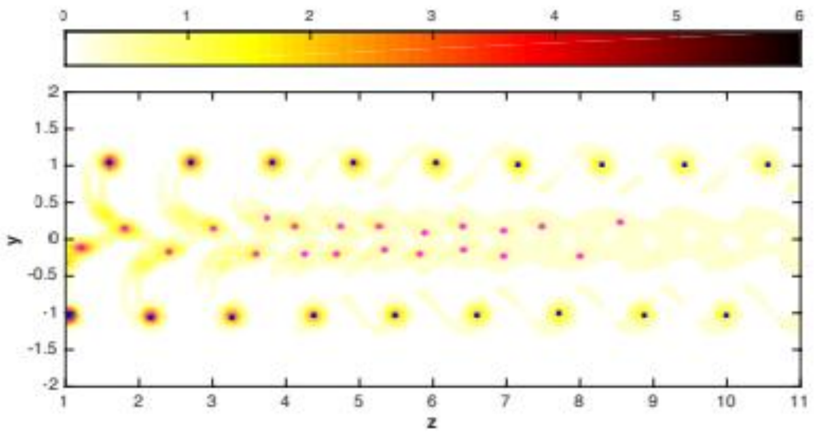

Figure 7 Contour of $|\varpi|$ in $yz-$ plane cut (SS1, Re1k). The blue squares represent the tip vortices while the pink stars are the root vortices.

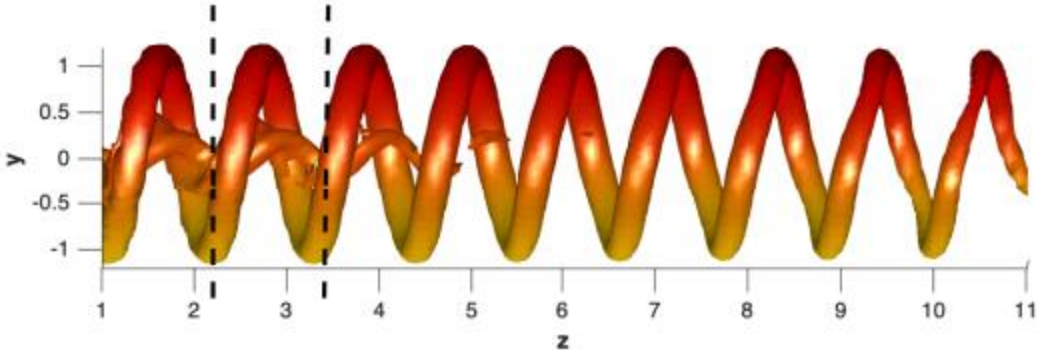

Figure 8: Isosurface of $|\varpi|$ from SS1, Re1k case for nine complete cycles with the dashed lines indicate the second complete cycle at $2.1 \leq z \leq 3.2$.

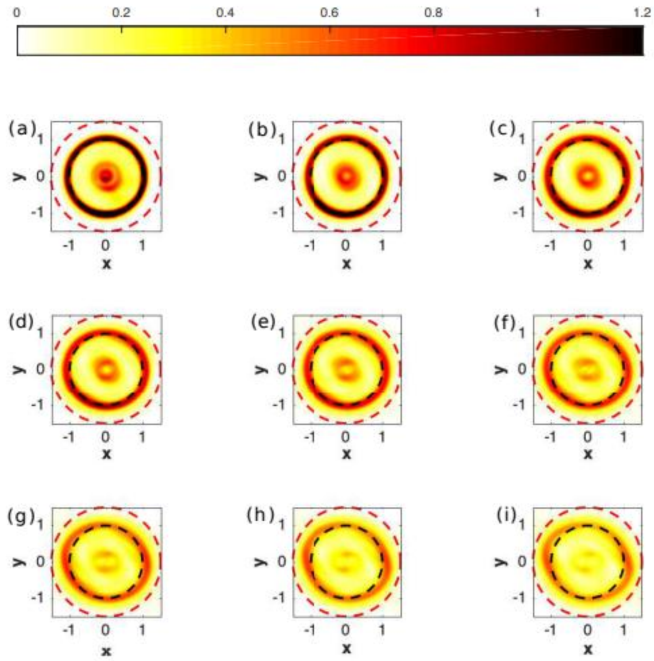

Figure 9: Contour of $|\varpi|$ (SS1, Re1k) at: (a) $1 \leq z \leq 2.1$ 1, (b) $2.1 \leq z \leq 3.2$, (c) $3.2 \leq z \leq 4.3$, (d) $4.3 \leq z \leq 5.4$, (e)$5.4 \leq z \leq 6.5$, (f) $6.5 \leq z \leq 7.6$, (g) $7.6 \leq z \leq 8.7$, (h) $8.7 \leq z \leq 9.8$, and (i) $9.8 \leq z \leq 10.9$.

Figure 10 shows the RMS values of the tip vortices. The deformation of the helical flow structure increased as the flow moves downstream except for both N cases. It shows how non-circular the helical flow is for every cycle and indirectly tells that the circular helical flow deformed to the ellipse at the end.

Figure 9, Figure 11, Figure 12, and Figure 13 were referred for a better visualization of how the helical flow shape distorts from its initial circular to an ellipse one in the process.

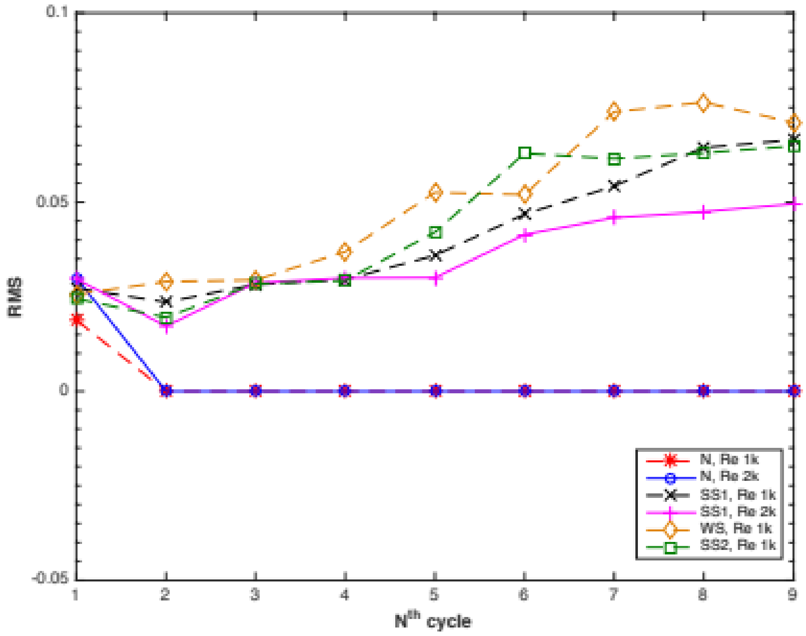

Figure 10: RMS Error of $|\varpi|$ from SS1, Re1k case for nine complete cycles with the dashed lines indicate the second complete cycle at $2.1 \leq z \leq 3.2$

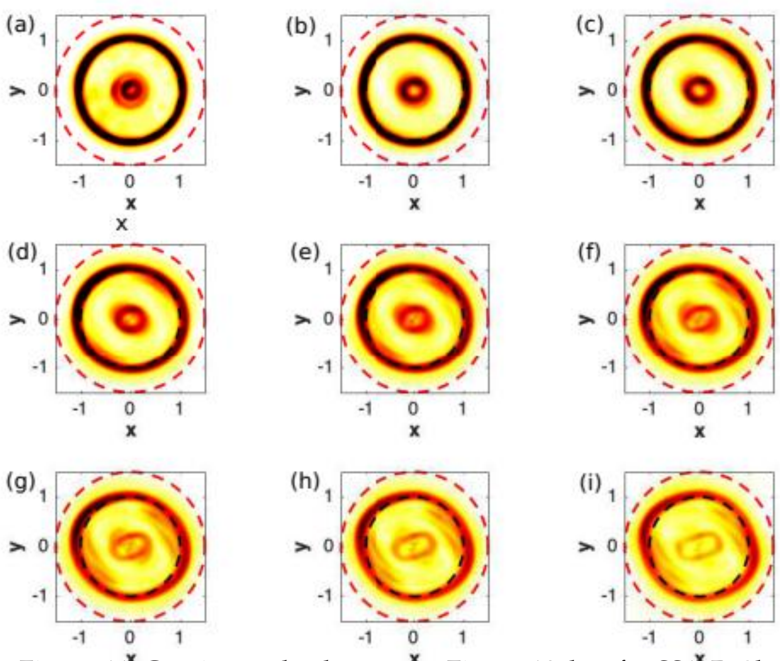

Figure 11: Caption and colormap as Figure 10, but for SS1, Re2k

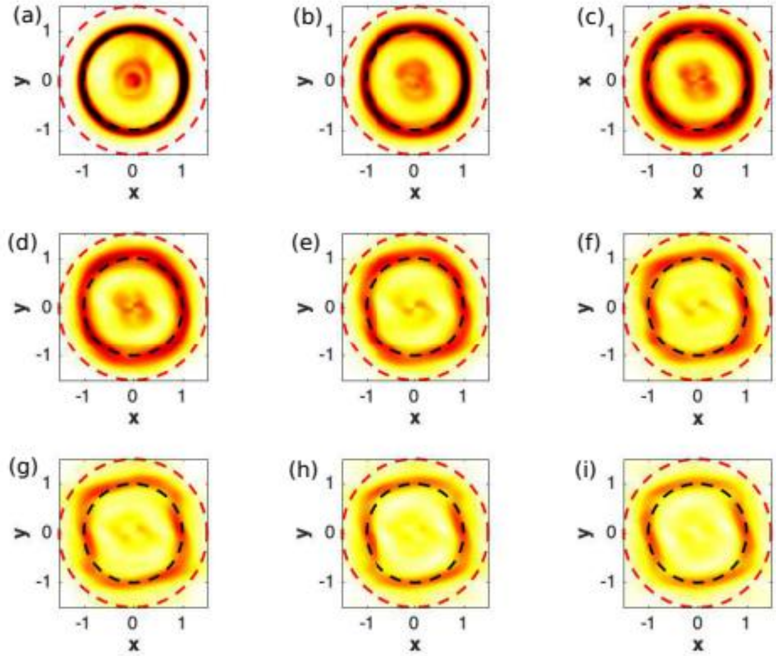

igure 12: Caption and colormap as Figure 10, but for WS, Re1k.

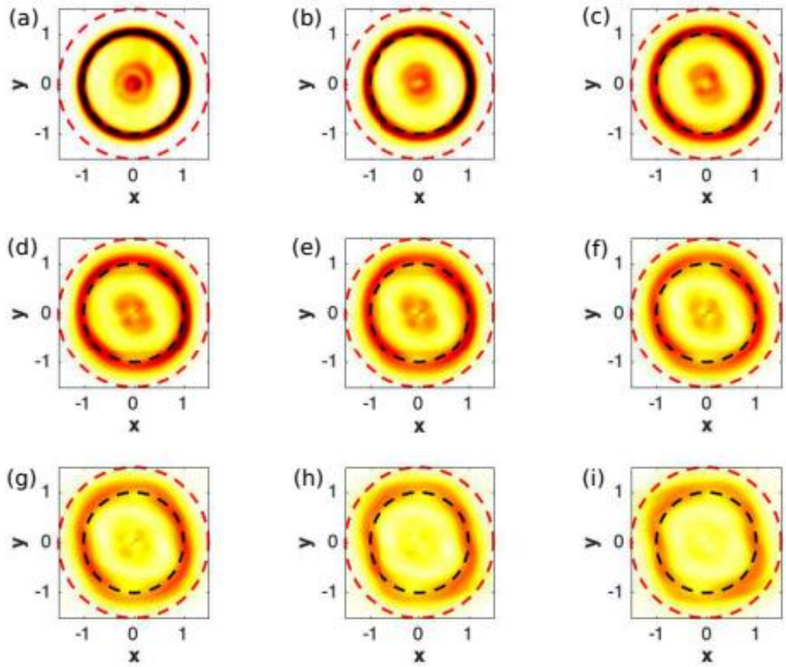

Figure 13: Caption and colormap as Figure 10, but for SS2, Re1k.

However, for the neutral cases (refer to the Figure 14), the helical flow started as non-circular as other cases before it went through the deformation into the perfect circle with zero RMS value. The blue and red line from Figure 10 support this observation when they both drop to zero in the second cycle and remain till the last.

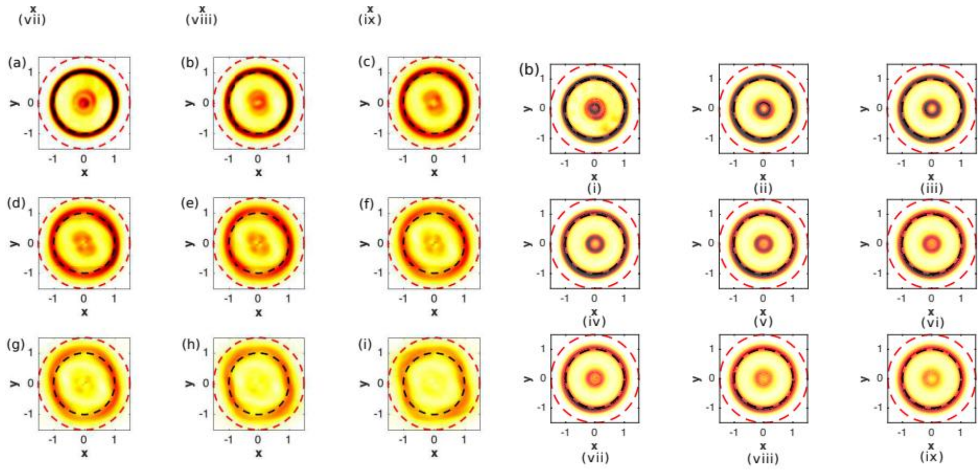

Figure 14: Caption and colormap as Figure 10, but for (a) N, Re1k, and (b) N, Re2k cases.

5.0 CONCLUSION

In this paper, the instantaneous helical wake behind a rotating blade of the six cases from three different atmospheric stratification conditions has been investigated. There is some interesting characteristics of the wake flow identified, such as its deformation/distortion, vorticity dynamics, vortex breakdown, and the centroid of the cores. All these analyses were focused only on the tip vortices. In the study of the deformation, the RMS values of the tip vortices were calculated to see how non-circular the helical flows are. The remaining characteristics mentioned earlier will be discussed in Part 2.

ACKNOWLEDGMENTS

The Authors also would like to thank Universiti Teknikal Malaysia Melaka (UTeM) for all the supports.

REFERENCES

[1] B. G. Green, E. A. Gillies, and R. E. Brown, "The Flow Field around a Rotor in Axial Descent", *Journal of Fluid Mechanics*, vol. 534, pp. 237–261, 2011.

[2] M. Felli, R. Camussi, F. di Felice, "Mechanisms of Evolution of the Propeller Wake in the Transition and Far Fields." *Journal of Fluid Mechanics*, vol. 682, pp. 5–53, 2011.

[3] M. O. L. Hansen, J. N. Sørensen, S. Voutsinas, N. Sørensen, H. A. Madsen, "State of the Art in Wind Turbine Aerodynamics and Aeroelasticity." Progress in Aerospace Sciences, vol. 42, pp. 285-330, 2006.

[4] J. K. Thorne. (2009). *Circular Wing Tip Trails*. [Online]. Available: http://www.vansairforce.com/community/showthread.php?t=47071

[5] *Wingtip Vortices*. [Online]. Available: https://www.wikiwand.com/en/Wingtip_vortices.

[6] CH. (2011). *Circular Wing Tip Trails*. [Online]. Available: https://atoptics.wordpress.com/tag/helicopter/

[7] FYFD. (2014). [Online]. Available: https://fyfluiddynamics.com/post/91050225974/smoke- released-from-theend-of-a-test-blade-shows

[8] M. Matin. "Predicting Interference Patterns between Offshore Wind Farms through

Wake Analysis." M.S thesis Carleton University Ottawa, Ontario, 2017.

[9] D. Maniaci, "Wakes and Rotors: The National Rotor Testbed." Sandia National Laboratories, 2014.

[10] B. Sanderse, "Aerodynamics of Wind Turbine Wakes – Literature Review." *Technical Report,* ECN-E-09-016, 2009.

[11] A. Crespo, J. Hernandez, and S. Frandsen, "Survey of Modelling Methods for Wind Turbine Wakes and Wind Farms", *Wind Energy*, vol. 2, pp. 1-24, 1999.

[12] M. Beychok. (2013). *Atmospheric Lapse Rate.* [Online]. Available: http://editors.eol.org/eoearth/wiki/Atmospheric_lapse _rate

[13] S. Sarmast, R. Dadfar Reza, R. F. Mikkelsen, P. Schlatter, S. Ivanell, J. N. Sørensen, and D. S. Henningson, "Mutual Inductance Instability of the Tip Vortices behind a Wind Turbine." *Journal of Fluid Mechanics*, vol. 755, pp. 705–731, 2014.

[14] A. K. M. F. Hussain, and M. Hayakawa, "Eduction of Large-scale Organized Structure in a Turbulent Plane Wake." *Journal of Fluid Mechanics*, vol. 180, 193, 1987.

[15] D. K. Bisset, R. A. Antonia, and L. W. B. Browne, "Spatial Organization of Large Structures in the Turbulent Far Wake of a Cylinder", *Journal of Fluid Mechanics*, vol. 218, 439, 1990.

[16] R. W. Metcalfe, F. Hussain, S. Menon, and M. Hakayawa, *Coherent Structures in a Turbent Mixing Layer: A Comparison between Numerical Simulations and Experiments*. In Turbulent Shear Flows 5 ed., (F. Durst, B. E. Launder, J. L. Lumley, F. W. Schmidt & J. H. Whitelaw): Springer. pp 110, 1985.

[16] M. O. L. Hansen, J. N. Sørensen, S. Voutsinas, N. Sørensen, H. A. Madsen, "State of the Art in Wind Turbine Aerodynamics and Aeroelasticity." *Progress in Aerospace Sciences,* vol. 42, pp. 285-330, 2006.